FISEVIER

Contents lists available at ScienceDirect

# **Composites Communications**

journal homepage: www.elsevier.com/locate/coco



#### **Short Communication**

# Detecting damage initiation in short fiber composites via in-situ X-ray tomography and digital volume correlation

Ronald F. Agyei<sup>a</sup>, Imad Hanhan<sup>a</sup>, Michael D. Sangid<sup>a,\*</sup>

a School of Aeronautics and Astronautics. Purdue University, 701 W. Stadium Ave. West Lafavette, IN 47906. USA

#### ARTICLE INFO

Keywords:
Incipient damage formation
DVC
Computer vision
3D microstructure
3D strain

#### ABSTRACT

In-situ X-ray tomography is an effective means for the acquisition of time-resolved 3D images of fiber reinforced composites during mechanical loading and deformation. However, the manual comparison of corresponding insitu X-ray images at successive loading instances to detect damage and its propagation is a time-consuming process. To improve the detection of damage using in-situ X-ray tomography, digital volume correlation (DVC), a full field 3D-strain technique that determines relative deformation between consecutive image volumes, was used. Specifically, regions of high strain were isolated from the heterogeneous strain computed from DVC within the microstructure and compared to manually detected damage. In this study, 59 out of 63 manually detected damage events, which included fiber breakage, micro-void nucleation, and fiber debonding, were within the search spaces of high strains beyond the 60th percentile threshold computed by DVC. Results of this study demonstrate the use of DVC as a tool to confine volumes of potential damage sites within the in-situ X-ray tomograms of composites to improve the efficiency of incipient damage detection.

### 1. Introduction

X-ray micro-computed tomography (µ-CT) is a qualitative and quantitative characterization technique, capable of determining a material's microstructure and defect structure [1]. The technique has been used to investigate multiple in-situ failure modes within symmetric cross ply laminated composites in monotonic [2] and cyclic [3] loading configurations. Hanhan et al. used in-situ tomography experiments coupled with a finite element simulation to show that regions of high hydrostatic stress correlated with incipient damage formation [4]. Typically, manual inspection of time lapse μ-CT images is used to detect microstructural and sub-volume damage evolution, but the process can be time consuming. Digital volume correlation (DVC) is a methodology to identify the displacement (and therefore strain) fields for a material across temporal states [5]. For instance, strain fields computed by DVC were used to quantify delamination [6] and transverse shear effects [7] in laminate composites. Yet, the precision of DVC in assisting microstructural damage detection in discontinuous fiber composites remains unclear. In this work, DVC was used to indicate regions of high strain during in-situ uni-axial tensile loading, and a methodology is presented to use the DVC results to identify regions of damage, thus providing a more efficient means for microstructural damage detection in comparison to the time-consuming traditional methods relying on manual inspection.

## 2. Methods

For this study, an injection molded, discontinuous glass-fiber reinforced polypropylene composite was machined into a dog-bone shaped sample with a grip diameter of 6.35 mm, a gauge section diameter of 2.4 mm, and a gauge height of 3.6 mm. X-ray  $\mu$ -CT characterization was performed on the specimen at Sector 2-BM of the Advanced Photon Source, Argonne National Laboratory. The synchrotron-based X-ray source provided quick data acquisition for in-situ loading, as well as the necessary phase contrast for detecting the fibers, matrix, and voids. An X-ray energy of 25 keV was used, and the specimen was rotated  $\pm 180^{\circ}$  at a velocity of  $0.5^{\circ}/s$ , with a sample-to-detector distance of 75 mm [8]. The tensile specimen was incrementally loaded in the Z direction via a screw-driven motor, and during interruptions in loading, X-ray μ-CT images of the full gauge cross-section were captured with a height of 1.8 mm. The sample was characterized 58 times until failure occurred within a region of the sample determined to be the ductile fracture zone; the engineering strain at failure,  $\varepsilon_f$ , 0.0042 (4.2%), was computed by comparing speckle pattern images on the specimen's gauge length (3.6

E-mail address: msangid@purdue.edu (M.D. Sangid).

<sup>\*</sup> Corresponding author.

mm in length) in VIC-2D.

X-ray projections were reconstructed to create serial sections of 1.3 μm pixel size grayscale images using Tomopy [9]. Afterwards, the glass fiber structure was reconstructed via a supervised iterative fiber reconstruction framework [10] (Fig. 1a) and the porosity was identified using Weka Segmentation [11] (Fig. 1b-d). ModLayer [12] was used to detect microstructural damage in the region of interest (referred to as the ductile fracture zone). For the purposes of this study, three epochs of the ductile fracture zone are shown (Fig. 1b-d, respectively) corresponding to pre-load  $(0\varepsilon_f)$ , at 30% of the macroscopic failure strain  $(0.3\varepsilon_f)$ , and at 99% of the macroscopic failure strain  $(0.99\varepsilon_f)$ . Damage was defined within the μ-CT volumes based on the appearance of well-defined dark intensity boundaries following the methodologies described in Ref. [13,14]. Sixty-three locations of incipient damage were manually detected at  $0.3\varepsilon_f$  (Fig. 1c) and were observed to coalesce resulting in catastrophic damage observed at  $0.99\varepsilon_f$  in Fig. 1d. Through manual inspection, the incipient damage locations at  $0.3\varepsilon_f$  were classified as either fiber breakage, micro-void nucleation, or fiber debonding.

A fast-Fourier transform based DVC algorithm [15] was used to calculate the corresponding strains from the greyscale  $\mu$ -CT sub-volumes, using a finite difference based calculation of the displacement field. In order to verify the choice of parameters and spatial resolution of the DVC results, a series of analyses were conducted on synthetic data. First, the fiber placement in a synthetic dataset was perturbed by a known amount or the entire volume was synthetically stretched, afterwards a parametric study was completed on the subset size and subset spacing. From this analysis, a subset size of 64 and subset spacing of 4 were determined suitable for this investigation, resulting in

a 1% difference between the DVC computed strain and the expected strain values in an approximate runtime of 6 h, using a desktop computer with an i7-4930 K CPU and 64 GB RAM. For the DVC analysis, the glass fibers within the microstructure are the fundamental features whose relative displacement, in general, results in the underlying strain distribution. Thus, spatial strain distribution inside a fiber cannot be measured, which is an inherent limitation of the DVC analysis. Next, a sensitivity analysis to the noise present in the  $\mu$ -CT data was conducted. Gaussian noise [16] was applied to the  $\mu$ -CT data at  $0\varepsilon_f$  and the subsequent DVC strains were computed to establish the expected error,  $\overline{\varepsilon_{zz}}$  =  $1*10^{-5}$ , of the analysis. For the remainder of this manuscript, the 3D strain map results refer to a DVC analysis conducted on the greyscale  $\mu$ -CT volume at 0.3 $ε_f$ . A threshold was applied to the DVC results to display the highest 97th percentile of strain (aligned to the loading direction) in the ductile fracture zone of the specimen (Fig. 1e). To define the DVC damage search spaces, a threshold value needs to be applied to the DVC strain results, which is critical to the precision and efficiency of the DVC-informed damage detection methodology, as explained in the next section.

#### 3. Results

Traditional, manual damage detection between two load states typically involves the following procedure: (1) inspection of the 2D slices of the tomographic volume (211 images in this case) comparing the reference state and the deformed state, (2) the confirmation of microstructural damage in each orthogonal plane, and (3) the marking (via point and click) of the boundaries of damage, using ModLayer [12], on each image. This process is very manually intensive and time

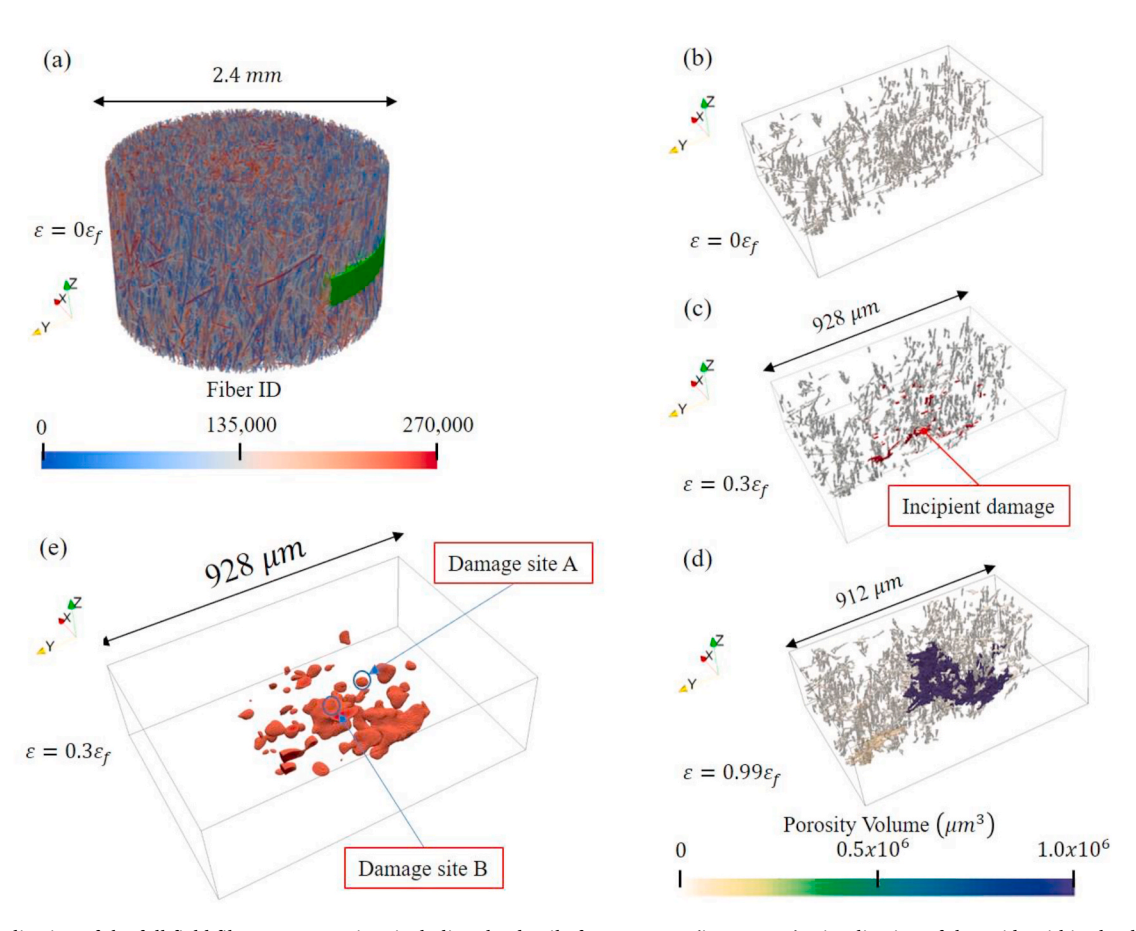


Fig. 1. (a) Visualization of the full field fiber reconstruction, including the ductile fracture zone (inset green); visualization of the voids within the ductile fracture zone at (b)  $0\varepsilon_f$ , (c)  $0.3\varepsilon_f$  (incipient damage overlaid in red), and (d)  $0.99\varepsilon_f$ , such that  $\varepsilon_f$  is the macroscopic failure strain of the specimen; (e) visualization of the DVC strain above the 97th percentile of  $\varepsilon_{zz}$  strains at the loading state corresponding to  $0.3\varepsilon_f$ . (For interpretation of the references to color in this figure legend, the reader is referred to the Web version of this article.)

consuming. The results are shown in Fig. 2 illustrating a 3D representation of the microstructural damage at two locations within the ductile failure zone, at  $0\varepsilon_f$  and  $0.3\varepsilon_f$ . At both locations (Fig. 2a and d), pre-existing pores (colored blue), with average volumes of 227  $\mu m^3$ , and fiber features, with average diameters of 10 µm, (colored according to their A<sub>33</sub> orientation, such that the orientation of the fibers are represented relative to the loading direction, please see Ref. [17] for more details) were present. After deformation at  $0.3\varepsilon_f$ , the damage evolved (colored in yellow) and was categorized as either fiber breakage (Fig. 2b) or microvoid nucleation (Fig. 2e). Sites of detected fiber breakage events had a mean diameter of 9.4 µm and the mean distance between broken fiber fragments was 6.3 µm. On the other hand, the mean volume of the detected sites of microvoid nucleation events was 428  $\mu m^3$  (equivalent to a sphere with diameter 9.4  $\mu m$ ). Both locations of manually detected damage overlapped with regions of high strains (97th percentile of strains corresponding to the red regions in Fig. 2c and f), hence a methodology is explored and discussed to use the regions of high strain determined by DVC as a means to reduce the search space for the identification of damage.

Fig. 3a shows a 2D slice of interest within the 3D ductile fracture zone, which has been tracked between  $0\varepsilon_f$ ,  $0.3\varepsilon_f$ , and  $0.5\varepsilon_f$  (Fig. 3c–e). The 3D strain map evaluated by DVC at  $0.3\varepsilon_f$  (Fig. 3b), where strain values above the 97th percentile of strains ( $\varepsilon_{zz} > 0.0269$ ), were retained as the search spaces for damage determination and outlined in red (Fig. 3f). At location 1 in Fig. 3f, the observed experimental damage (matrix cracking and fiber breakage denoted with black marks) fall within the DVC search space. The same observation was made for another instance of fiber breakage (location 2) and micro-void nucleation (location 3). These observations demonstrate that the downselected search spaces, based on regions of high strain informed by the DVC analysis, can be used to aid visual inspection for damage detection. Buljac et al. introduced a method using the grey-level residual field to detect damage based off discontinuities between the DVC displacement field and the original greyscale image [18]. As shown in Fig. 3g, the grey-level residual field is displayed relative to the damage sites. Given

the complexity of the microstructural features, the grey-level residual field could not distinguish extreme values with sites of observed damage in the present sample. The correlation coefficient between the thresholded DVC search space (in Fig. 3b) and the observed sites of damage is 0.1081, which is significantly higher than the correlation coefficient of 0.007 between the grey-level residual field (in Fig. 3g) and the observed sites of damage.

Lastly, the precision and efficiency of this approach is contingent upon the appropriate choice of the threshold value of strain relative to the distribution of strains computed by the DVC analysis. To evaluate the detection of damage as a function of the localized strain threshold, search spaces confined within the 60th to the 99.9th percentile of the strain distribution in increments of 0.1 were assessed. The accuracy of the DVC informed method to detect damage was defined when the locations of manually detected damage were within the DVC search spaces. As shown in Fig. 4a, at the 60th percentile, a 93% success rate in damage detection (equivalent to 59 out of 63 damage locations) was observed, yet at increasing percentile thresholds, the DVC informed method of damage identification was less successful and captured fewer damage sites. This is due to the fact that at increasing percentile thresholds, search spaces became smaller in volume, with damage events increasingly occurring next to, but outside, the boundary DVC informed search spaces.

Additionally, the precision of the DVC informed method of damage detection was quantified by identifying the damage volume relative to its corresponding DVC search space. Fig. 4b shows that higher percentile strain thresholds resulted in smaller search spaces, thereby expediting the manual inspection of damage sites via an exponentially increasing trend (albeit at the expense of overall accuracy, as previously shown in Fig. 4a). The DVC search space that did not necessarily correspond to the observed damage sites were usually of negligible volume overall. To illustrate this, at the 60th percentile, 11 search spaces were computed. One of the search spaces (of volume 0.0120 mm³) contained all of the detected damage sites, while the other ten search spaces (which all had volumes less than 0.0001 mm³) did not contain any damage sites. The

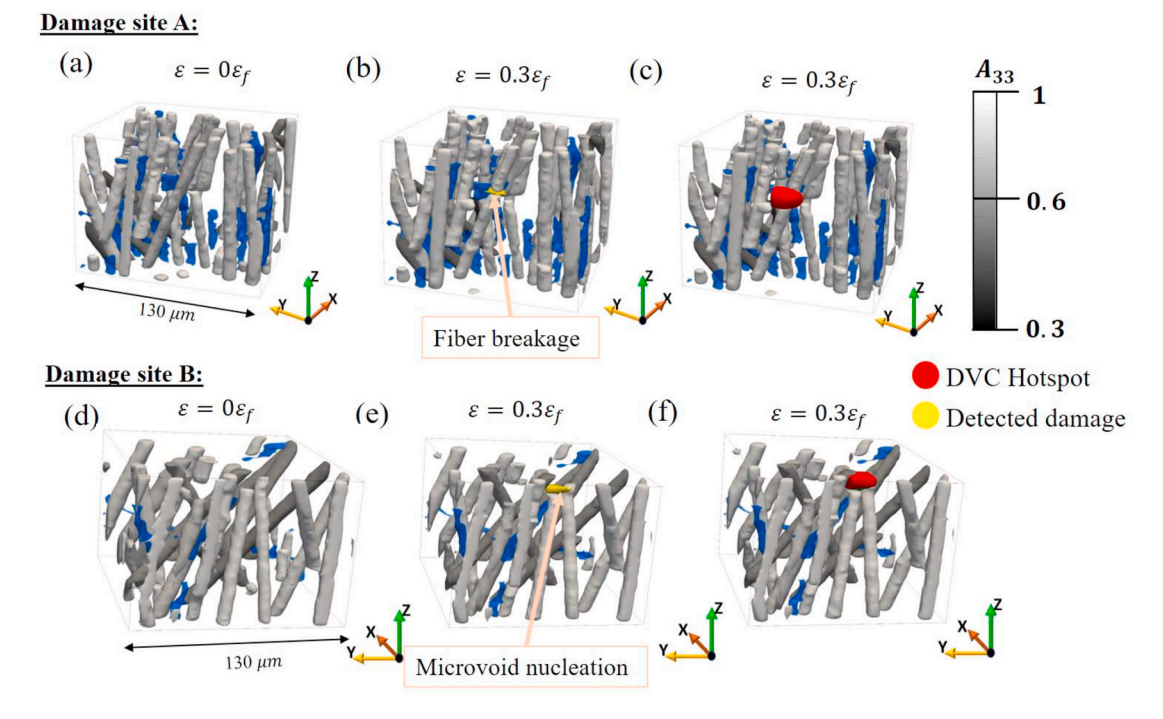


Fig. 2. Damage detection at two separate locations in the microstructure (indicated as sites A and B in Fig. 1e): 3D visualization of the microstructural fibers (fibers are shaded relative to their orientation with respect to the loading axis,  $A_{33}$ ) and manufacturing pores (blue) at the unloaded state (a and d). At  $0.3\varepsilon_f$ , the location of damage events, fiber breakage and microvoid nucleation, are shown in yellow (b and e, respectively). At  $0.3\varepsilon_f$ , the DVC analysis depicts regions of high strain (97th percentile of  $\varepsilon_{zz}$ ), as shown in red (c and f). (For interpretation of the references to color in this figure legend, the reader is referred to the Web version of this article.)

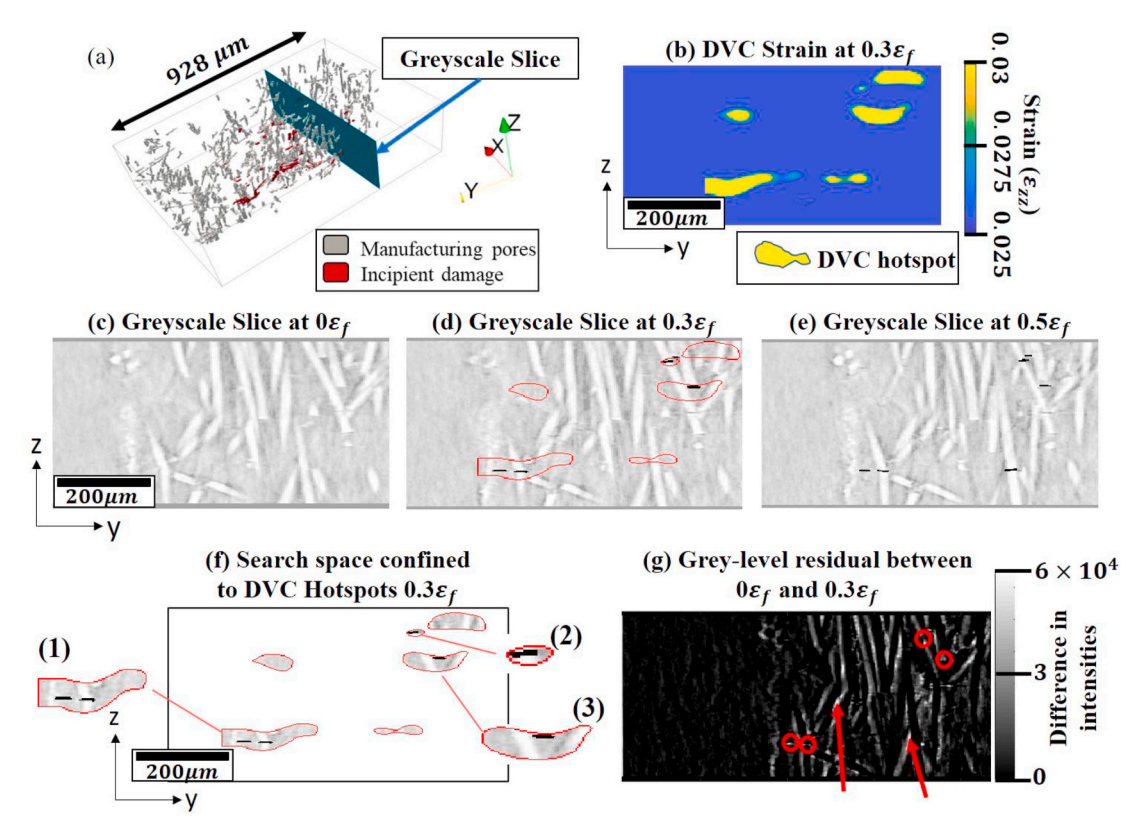


Fig. 3. (a) 3D view of a region of interest within then ductile fracture zone, denoting pores present after manufacturing, as well as pores formed from incipient damage. A 2D grayscale slice is shown within this 3D region for further investigation. (b) DVC computed strain at  $0.3\varepsilon_f$ . A 2D view of the greyscale slice of the microstructure at (c)  $0\varepsilon_f$ , (d)  $0.3\varepsilon_f$  with the regions above the 97th percentile threshold of strains outlined in red and damage sites indicated in black, and (e)  $0.5\varepsilon_f$  with damage sites indicated in black. (f) Search spaces confined to regions denoted by the 97th percentile of strains, which enclosed the following damage events: (1) fiber breakage and matrix cracking, (2) fiber breakage, and (3) microvoid nucleation. (g) Grey-level residual fields with circle insets indicating locations of observed incipient damage and arrows indicating locations of non-damage identified as discontinuities due to the local fluctuation in intensities. (For interpretation of the references to color in this figure legend, the reader is referred to the Web version of this article.)

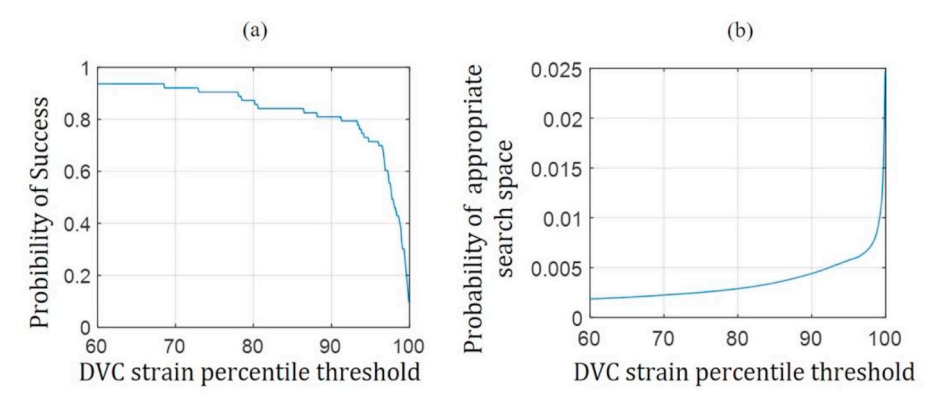


Fig. 4. (a) Probability of success (ratio of successfully detected damage sites within the DVC informed search space to the total number of experimentally detected damage sites) versus the selected percentile threshold of the DVC strain distribution. (b) Probability of appropriate search space (ratio of the volume of the experimentally detected damage site to the enclosed volume defined by the region of strains higher than the denoted DVC threshold value) versus the selected percentile threshold of the DVC strain distribution.

trends shown in Fig. 4 indicate that when using DVC search spaces to confine the images for manual damage detection, a higher strain threshold will result in more precise search spaces, however, it will also lead to a lower number of total detected damage sites. Hence depending on the resolution of the DVC analysis, the damage mechanisms present, and the material's microstructure, a balance must be defined between efficiency and accuracy of the DVC informed damage identification procedure introduced in this work.

#### 4. Conclusion

In this work, locations of incipient damage identified via X-ray

tomography (of a short fiber composite microstructure) corresponded with regions of high strains determined through DVC analysis. Specifically, this work quantified the correlation between sites of experimental incipient damage and high strains as computed by DVC, as well as the ability to successfully detect damage based on the selected threshold value of strain from the distribution computed via DVC. The analysis investigated strain thresholds ranging from the 60th to the 99.9th percentile, which showed success rates as high as 93% (compared to the expected damage sites from experimental observations of damage). A methodology is proposed to use the resulting DVC results, in order to streamline the traditional time-consuming manual process of incipient damage detection in fiber-reinforced composites.

- Conduct a sensitivity analysis to select the optimum subset size and spacing for the DVC analysis on synthetically deformed tomography images, which will also quantify the uncertainty values in the analysis.
- 2. For the time-lapse tomography dataset, apply a DVC analysis to compute the 3D strain field in the full microstructure.
- On a small sub-volume, use a segmentation tool for visualizing and classifying 3D data, such as ModLayer [12], to threshold and manually segment detected damage sites.
- 4. Conduct, on the small sub-volume, a strain threshold sensitivity analysis to determine an appropriate strain threshold that balances the success rate and precision (as described in Fig. 4).
- 5. Apply the appropriate strain threshold (based on the small subvolume) to the full microstructure, thereby reducing the search spaces for the identification of damage.
- Use ModLayer, to visually inspect the confined search spaces for the identification of damage events that occurred in the tomography images.

The DVC-informed damage detection methodology presented in this paper is applicable to a general class of composite materials, while the specific analysis is dependent on (i) the resolution of the DVC strain fields produced and (ii) the damage mechanisms within the material. First, DVC tracks the secondary phases (fibers in the present case) to identify the displacement field evolution. For the necessary highresolution DVC field, the tomograms should contain a dense configuration of features to track, which requires a sufficient volume fraction of secondary phases, distinct phase contrast between phases, and high spatial resolution in the tomograms. Second, identifying a suitable strain threshold to denote the potential damage sites requires the procedure outlined in this paper to be repeated based on the configuration of interest. The outcome will depend on the resolution and heterogeneity of the DVC field, which are dependent on the active damage mechanisms, prevalence of damage (in terms of uniformity or sparseness), and the interaction of damage mechanisms, each of which are dependent on the loading configuration on the material. Overall, employing such a DVCinformed methodology, compared to visual inspection of the full tomography volume, can save engineers time and computational resources in their efforts to detect 3D damage events in large time-lapse tomography volumes.

#### CRediT authorship contribution statement

Ronald F. Agyei: Data curation, Formal analysis, Investigation, Software, Validation, Visualization, Writing - original draft. Imad Hanhan: Conceptualization, Methodology, Validation, Visualization, Writing - review & editing. Michael D. Sangid: Conceptualization, Methodology, Project administration, Funding acquisition, Resources, Supervision, Validation, Visualization, Writing - review & editing.

# Declaration of competing interest

The authors declare that they have no known competing financial interests or personal relationships that could appear to influence the work reported in this paper.

### Acknowledgements

Support for this work was provided by the National Science Foundation CMMI MoM, Award No. 1662554 (Program Manager Dr. Siddiq Qidwai). The authors would like to thank Dr. Francesco de Carlo and Pavel Shevchenko from Argonne National Laboratory for providing the

experimental set-up and expertise necessary during the X-ray tomography data acquisition. The material used in this study was provided by Dr. Alan Wedgewood. The authors would also like to thank Mohak Patel, Alexander Landauer, and Dr. Christian Franck of the University of Wisconsin, Madison for their helpful and insightful discussions with regards the DVC algorithm used in this work. This research used resources of the Advanced Photon Source, a U.S. Department of Energy (DOE) Office of Science User Facility operated for the DOE Office of Science by Argonne National Laboratory under Contract No. DE-AC02-06CH11357.

#### References

- [1] E. Maire, P.J. Withers, Quantitative X-ray tomography, Int. Mater. Rev. 59 (2014) 1–43, https://doi.org/10.1179/1743280413Y.0000000023.
- [2] A.E. Scott, M. Mavrogordato, P. Wright, I. Sinclair, S.M. Spearing, In situ fibre fracture measurement in carbon-epoxy laminates using high resolution computed tomography, Compos. Sci. Technol. 71 (2011) 1471–1477, https://doi.org/ 10.1016/j.compscitech.2011.06.004.
- [3] S.C. Garcea, M.N. Mavrogordato, A.E. Scott, I. Sinclair, S.M. Spearing, Fatigue micromechanism characterisation in carbon fibre reinforced polymers using synchrotron radiation computed tomography, Compos. Sci. Technol. 99 (2014) 23–30, https://doi.org/10.1016/j.compscitech.2014.05.006.
- [4] I. Hanhan, R.F. Agyei, X. Xiao, M.D. Sangid, Predicting microstructural void nucleation in discontinuous fiber composites through coupled in-situ X-ray tomography experiments and simulations, Sci. Rep. 10 (2020) 1–8, https://doi. org/10.1038/s41598-020-60368-w.
- [5] B.K. Bay, T.S. Smith, D.P. Fyhrie, M. Saad, Digital volume correlation: threedimensional strain mapping using X-ray tomography, Exp. Mech. 39 (1999) 217–226, https://doi.org/10.1007/BF02323555.
- [6] P. Lecomte-Grosbras, J. Réthoré, N. Limodin, J.F. Witz, M. Brieu, Three-Dimensional investigation of free-edge effects in laminate composites using X-ray tomography and digital volume correlation, Exp. Mech. 55 (2015) 301–311, https://doi.org/10.1007/s11340-014-9891-1.
- [7] R. Brault, A. Germaneau, J.C. Dupré, P. Doumalin, S. Mistou, M. Fazzini, In-situ analysis of laminated composite materials by X-ray micro-computed tomography and digital volume correlation, Exp. Mech. 53 (2013) 1143–1151, https://doi.org/ 10.1007/s11340-013-9730-9.
- [8] I. Hanhan, R. Agyei, X. Xiao, M.D. Sangid, Comparing non-destructive 3D X-ray computed tomography with destructive optical microscopy for microstructural characterization of fiber reinforced composites, Compos. Sci. Technol. 184 (2019) 107843, https://doi.org/10.1016/j.compscitech.2019.107843.
- [9] D. Gurrsoy, F. De Carlo, X. Xiao, C. Jacobsen, TomoPy: a framework for the analysis of synchrotron tomographic data, J. Synchrotron Radiat. 21 (2014) 1188–1193, https://doi.org/10.1107/S1600577514013939.
- [10] R.F. Agyei, M.D. Sangid, A supervised iterative approach to 3D microstructure reconstruction from acquired tomographic data of heterogeneous fi brous systems, Compos. Struct. 206 (2018) 234–246, https://doi.org/10.1016/j. compstruct.2018.08.029.
- [11] I. Arganda-Carreras, V. Kaynig, C. Rueden, K.W. Eliceiri, J. Schindelin, A. Cardona, H.S. Seung, Trainable Weka Segmentation: a machine learning tool for microscopy pixel classification, Bioinformatics 33 (2017) 2424–2426, https://doi.org/ 10.1093/bioinformatics/btx180.
- [12] I. Hanhan, M.D. Sangid, ModLayer: a MATLAB GUI drawing segmentation tool for visualizing and classifying 3D data, Integr. Mater. Manuf. Innov. 8 (2019) 468–475, https://doi.org/10.1007/s40192-019-00160-5.
- [13] P.J. Withers, M. Preuss, Fatigue and damage in structural materials studied by X-ray tomography, Annu. Rev. Mater. Res. 42 (2012) 81–103, https://doi.org/10.1146/annurev-matsci-070511-155111.
- [14] C.M. Loeffler, Y. Qiu, B. Martin, W. Heard, B. Williams, X. Nie, Detection and segmentation of mechanical damage in concrete with X-Ray microtomography, Mater. Char. 142 (2018) 515–522, https://doi.org/10.1016/j. matchar.2018.06.018.
- [15] E. Bar-Kochba, J. Toyjanova, E. Andrews, K.S. Kim, C. Franck, A fast iterative digital volume correlation algorithm for large deformations, Exp. Mech. 55 (2015) 261–274, https://doi.org/10.1007/s11340-014-9874-2.
- [16] P. Tu, Y. Bai, W. Xu, B. Dong, S. Ye, Q. Yang, Y. Zhou, Digital volume correlation in an environment with intensive salt-and-pepper noise and strong monotonic nonlinear distortion of light intensity, Opt. Appl. 47 (2017) 209–223, https://doi. org/10.5277/oa170204.
- [17] S.G. Advani, C.L. Tucker, The use of tensors to describe and predict fiber orientation in short fiber composites, J. Rheol. (N. Y. N. Y). 31 (1987) 751–784, https://doi.org/10.1122/1.549945.
- [18] A. Buljac, C. Jailin, A. Mendoza, J. Neggers, T. Taillandier-Thomas, A. Bouterf, B. Smaniotto, F. Hild, S. Roux, Digital volume correlation: progress and challenges, Conf. Proc. Soc. Exp. Mech. Ser. C (2020) 113–115, https://doi.org/10.1007/978-3-030-30009-8 17.